

# Effective time-frequency characterization of Lamb wave dispersion in plate-like structures with non-reflecting boundaries

Zijian Wang<sup>\*1</sup>, Pizhong Qiao<sup>2a</sup> and Binkai Shi<sup>3b</sup>

<sup>1</sup>Department of Dam Safety Management, Nanjing Hydraulic Research Institute, 225 Guangzhou Road, Nanjing, 210029, China

<sup>2</sup>Department of Civil and Environmental Engineering, Washington State University, Sloan Hall 117, Pullman, WA, 99164-2910, USA

<sup>3</sup>School of Mechanics and Materials, Hohai University, Nanjing, 210098, China

(Received May 9, 2017, Revised November 24, 2017, Accepted January 11, 2018)

**Abstract.** Research on Lamb wave-based damage identification in plate-like structures depends on precise knowledge of dispersive wave velocity. However, boundary reflections with the same frequency of interest and greater amplitude contaminate direct waves and thus compromise measurement of Lamb wave dispersion in different materials. In this study, non-reflecting boundaries were proposed in both numerical and experimental cases to facilitate time-frequency characterization of Lamb wave dispersion. First, the Lamb wave equations in isotropic and laminated materials were analytically solved. Second, the non-reflecting boundaries were used as a series of frames with gradually increased damping coefficients in finite element models to absorb waves at boundaries while avoiding wave reflections due to abrupt property changes of each frame. Third, damping clay was sealed at plate edges to reduce the boundary reflection in experimental test. Finally, the direct waves were subjected to the slant-stack and short-time Fourier transformations to calculate the dispersion curves of phase and group velocities, respectively. Both the numerical and experimental results suggest that the boundary reflections are effectively alleviated, and the dispersion curves generated by the time-frequency analysis are consistent with the analytical solutions, demonstrating that the combination of non-reflecting boundary and time-frequency analysis is a feasible and reliable scheme for characterizing Lamb wave dispersion in plate-like structures.

**Keywords:** Lamb wave dispersion; non-reflecting boundary; slant-stack transformation; short-time fourier transformation; classical laminated plate theory; plate-like structures

## 1. Introduction

Deterioration of engineering structures throughout their service lives is a significant problem (Yi *et al.* 2011, 2013). Current inspections of engineering structures are usually based on various nondestructive testing (NDT) methods to provide warning of catastrophic failure. The Lamb wave-based method has exhibited remarkable advantages in damage identification for plate-like structures (Wang and Qiao 2017, Wang *et al.* 2017), since Lamb waves can propagate over a long distance (Qiu *et al.* 2013) and are highly sensitive to various forms of damage (Wang *et al.* 2015, Wang *et al.* 2016, Tao *et al.* 2017). The function modes of transducers in Lamb wave-based damage identification include the pulse-echo and pitch-catch modes (Giurgiutiu 2011). The pulse-echo mode takes the time-of-flight, which is the time interval between excitation and damage reflection, to multiply the Lamb wave velocity to determine distance between damage and transducer. On

the other hand, the pitch-catch mode investigates time delay of a direct wave to detect damage on the path between transducers or nearby. To this end, both modes require precise knowledge of Lamb wave velocity to produce accurate damage localization. However, the dispersive nature of Lamb waves leads to different velocities of individual frequency, impeding implementation of Lamb waves in damage identification.

The analytical characterization of Lamb wave dispersion has been examined (He *et al.* 2013). In isotropic materials, the Lamb wave equation is solved based on the theory of elasticity by considering the traction-free boundary condition. In laminated materials, wave scattering and mode conversion at the interface in plies complicate the characterization of Lamb wave dispersion. Thus, the transfer (Wang and Yuan 2007) and global (Pant *et al.* 2014) matrix methods have been adopted to coordinate the displacement and stress at the interface in plies to calculate the dispersion curve of Lamb waves.

Since the analytical solutions can only be derived in simple scenarios, finite element (FE) modeling has been adopted to aid in the study of Lamb wave dispersion in complex cases (Hong *et al.* 2014, Poddar and Giurgiutiu 2016a, b). The measurements of dispersion curves, which show the relationship between frequency and wave velocity, are mainly based in the pitch-catch mode via a series of transducers. However, the plate edges cause strong wave reflection and contaminate the signals received by

---

\*Corresponding author, Ph.D.

E-mail: [zijianwang@nhri.cn](mailto:zijianwang@nhri.cn)

<sup>a</sup> Professor

E-mail: [Qiao@wsu.edu](mailto:Qiao@wsu.edu)

<sup>b</sup> Ph.D. Student

E-mail: [hhusbk2009@hhu.edu.cn](mailto:hhusbk2009@hhu.edu.cn)

transducers. Since these boundary reflections have the same frequency and greater amplitude than the direct waves, it is difficult to separate the direct waves in order to calculate the wave velocities relating to different frequencies. To prevent the boundary reflections from compromising the measurement of dispersion curves, it is desirable to develop non-reflecting boundaries to keep the area of measurement clean. The present non-reflecting boundaries include infinite elements (Liu and Jerry 2003), dashpot supports (Hosseini *et al.* 2013), spring-damper elements (Shen and Giurgiutiu 2015), and damping sections (Drozd *et al.* 2006).

In this study, non-reflecting boundaries were developed in both numerical finite element (FE) model and experiment to alleviate boundary reflections and facilitate measurement of dispersion curves. The analytical solutions of the Lamb wave equation for isotropic and laminated materials were formulated as the benchmarks of the following measurement in the first place. Subsequently, non-reflecting boundaries were designed in the FE model and applied in the experiment as damping frames to absorb waves at plate edges. Finally, the direct waves were clearly received by transducers to calculate the dispersion curves of phase and group velocities through the slant-stack (Ambrozinski *et al.* 2014) and short-time Fourier transformations (Niethammer *et al.* 2000), respectively. Both the numerical and experimental results agree well with the analytical solutions, demonstrating that the combination of non-reflecting boundary and time-frequency analysis is a feasible and reliable scheme for characterizing Lamb wave dispersion in plate-like structures.

## 2. Analytical solution of the Lamb wave dispersion

Elastic waves in infinite isotropic materials consist of three decoupled bulk waves, i.e., longitudinal, shear vertical, and shear horizontal waves. For thin-walled isotropic materials, whose thickness has the same scale as the wave length, the bulk waves hit the top and bottom surfaces of the structure and get reflected, merging to generate Lamb waves that propagate within the structure. In this process, the longitudinal and shear vertical waves couple to two vibration modes (i.e., the symmetric and anti-symmetric modes) of Lamb waves, leaving the shear horizontal wave decoupled. In this section, the dispersion curves of Lamb waves in isotropic and laminated materials are analytically solved.

### 2.1 Isotropic materials

According to the displacement potential or partial wave method (Rose 2004), the longitudinal and shear vertical waves are decoupled from the Lamb wave equations, forming the Rayleigh-Lamb equation

$$\frac{\tan ph}{\tan qh} = - \left[ \frac{4k^2 pq}{(k^2 - q^2)^2} \right]^{\pm 1} \quad (1)$$

$$p = \sqrt{\left(\frac{\omega}{c_L}\right)^2 - (k)^2} \quad q = \sqrt{\left(\frac{\omega}{c_T}\right)^2 - k^2} \quad (2)$$

$$k = \frac{\omega}{c_p} \quad c_L = \frac{\lambda + 2\mu}{\rho} \quad c_T = \frac{\mu}{\rho} \quad (3)$$

where  $\omega$  is the circular frequency;  $c_p$  is the phase velocity;  $c_L$  is the velocity of the longitudinal wave;  $c_T$  is the velocity of the shear vertical wave;  $h$  is the half thickness of the plate;  $k$  is the wavenumber;  $\lambda$  and  $\mu$  are the Lamé constants; and +1 and -1 represent the symmetric and anti-symmetric modes, respectively. As an example, the dispersion curve of phase velocity is presented in Fig. 1(a) for an aluminum plate whose material properties are shown in Table 1. Due to the dispersive nature, the phase velocity varies according to frequency. In addition, the dispersion curve of group velocity, which shows the average velocity of the whole wave packet containing various frequency contents, is plotted in Fig. 1(b)

$$c_g = \frac{c_p^2}{c_p - fh \frac{d(c_p)}{d(fh)}} \quad (4)$$

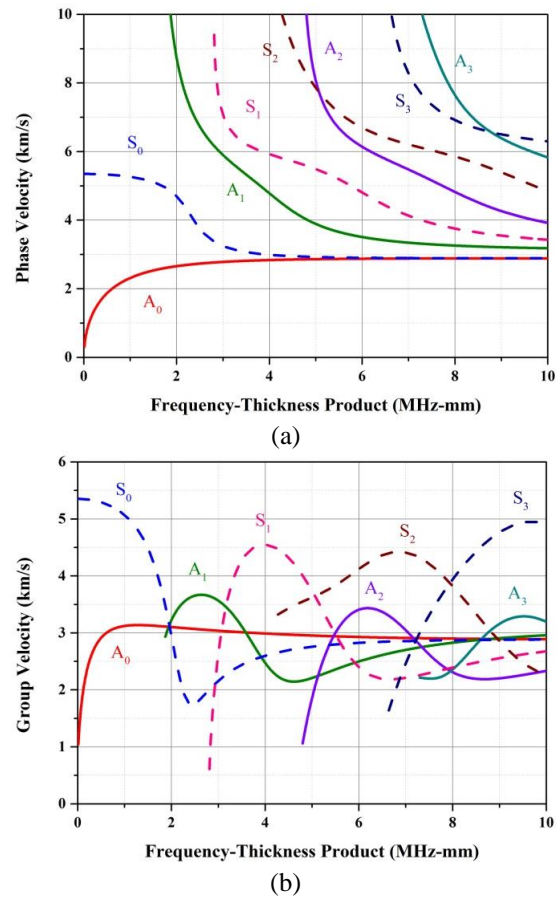


Fig. 1 Dispersion curves of aluminum plate: (a) phase velocity and (b) group velocity

Table 1 Material properties of aluminum plate

Young's modulus	Poisson's ratio	Density
68.9 GPa	0.33	2700 kg/m <sup>3</sup>

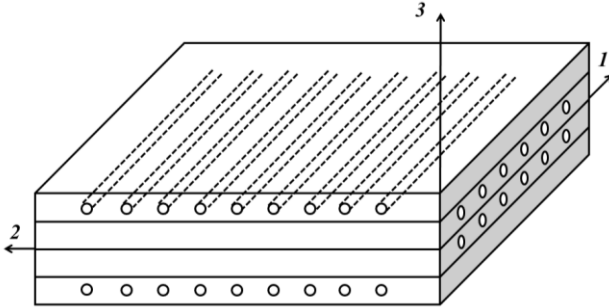


Fig. 2 Model of the laminated material

## 2.2 Laminated materials

Considering the symmetric  $N$ -layered laminates illustrated in Fig. 2, the fiber-reinforced plies on the  $x_1$ - $x_2$  plane are perfectly bonded at interfaces and stacked in the  $x_3$  direction. When the waves propagate off the symmetry on the  $x_1$ - $x_2$  plane, the whole laminates are characterized as monoclinic material about the mid-plane.

According to the theory of elasticity, the equilibrium equations are as follows

$$\begin{aligned} \frac{\partial \sigma_{11}}{\partial x_1} + \frac{\partial \sigma_{12}}{\partial x_2} + \frac{\partial \sigma_{13}}{\partial x_3} &= \rho \frac{\partial^2 u_1}{\partial t^2} \\ \frac{\partial \sigma_{12}}{\partial x_1} + \frac{\partial \sigma_{22}}{\partial x_2} + \frac{\partial \sigma_{23}}{\partial x_3} &= \rho \frac{\partial^2 u_2}{\partial t^2} \\ \frac{\partial \sigma_{13}}{\partial x_1} + \frac{\partial \sigma_{23}}{\partial x_2} + \frac{\partial \sigma_{33}}{\partial x_3} &= \rho \frac{\partial^2 u_3}{\partial t^2} \end{aligned} \quad (5)$$

where  $\rho$  is the density of ply. Applying the equivalent matrix to simplify the laminate as homogeneous material

$$[C] = \frac{\sum_{k=1}^N [\bar{Q}]_k (x_3^k - x_3^{k-1})}{2h} \quad (6)$$

where  $[\bar{Q}]_k$  is the global stiffness matrix of the  $k$ -th layer.

Due to the symmetry of laminates, the equivalent matrix is in the form of monoclinic materials

$$\begin{bmatrix} \sigma_{11} \\ \sigma_{22} \\ \sigma_{33} \\ \sigma_{23} \\ \sigma_{13} \\ \sigma_{12} \end{bmatrix} = \begin{bmatrix} C_{11} & C_{12} & C_{13} & 0 & 0 & C_{16} \\ C_{12} & C_{22} & C_{23} & 0 & 0 & C_{26} \\ C_{13} & C_{23} & C_{33} & 0 & 0 & C_{36} \\ 0 & 0 & 0 & C_{44} & C_{45} & 0 \\ 0 & 0 & 0 & C_{45} & C_{55} & 0 \\ C_{16} & C_{26} & C_{36} & 0 & 0 & C_{66} \end{bmatrix} \begin{bmatrix} \varepsilon_{11} \\ \varepsilon_{22} \\ \varepsilon_{33} \\ \gamma_{23} \\ \gamma_{13} \\ \gamma_{12} \end{bmatrix} \quad (7)$$

To define a homogenous plane wave, all the displacements are assumed to be uniform over the wavefront.

$$u_n = U_n e^{ik(x_1 + \alpha x_3 - c_p t)} \quad (n=1,2,3) \quad (8)$$

The strain-displacement relationship is as follows

$$\begin{aligned} \varepsilon_{11} &= \frac{\partial u_1}{\partial x_1} & \varepsilon_{22} &= \frac{\partial u_2}{\partial x_2} & \varepsilon_{33} &= \frac{\partial u_3}{\partial x_3} \\ \varepsilon_{12} &= \frac{\partial u_1}{\partial x_2} + \frac{\partial u_2}{\partial x_1} & \varepsilon_{23} &= \frac{\partial u_2}{\partial x_3} + \frac{\partial u_3}{\partial x_2} & \varepsilon_{13} &= \frac{\partial u_1}{\partial x_3} + \frac{\partial u_3}{\partial x_1} \end{aligned} \quad (9)$$

and substituting Eqs. (7) and (8) into Eqs. (5) and (9) leads to the following

$$K_{mn}(\alpha) U_n = 0 \quad (m,n=1,2,3) \quad (10)$$

where

$$\begin{aligned} K_{11} &= C_{11} + C_{55} \alpha^2 - \rho c_p^2 & K_{12} &= C_{16} + C_{45} \alpha^2 & K_{13} &= (C_{13} + C_{55}) \alpha \\ K_{22} &= C_{66} + C_{44} \alpha^2 - \rho c_p^2 & K_{23} &= (C_{36} + C_{45}) \alpha & K_{33} &= C_{55} + C_{33} \alpha^2 - \rho c_p^2 \end{aligned} \quad (11)$$

The nontrivial solutions of Eq. (10) require the determinant of matrix  $K_{mn}$  to be zero, further leading to a polynomial equation

$$\alpha^6 + A_1 \alpha^4 + A_2 \alpha^2 + A_3 = 0 \quad (12)$$

where the coefficient  $A$  is listed in Appendix A. There are six roots for Eq. (12) with unique properties as

$$\alpha_2 = -\alpha_1 \quad \alpha_4 = -\alpha_3 \quad \alpha_6 = -\alpha_5 \quad (13)$$

$\alpha_1$ ,  $\alpha_2$ , and  $\alpha_3$  represent the roots with a positive imaginary part, while  $\alpha_4$ ,  $\alpha_5$ , and  $\alpha_6$  represent the roots with a negative imaginary part. To normalize the displacement, the displacement ratios are defined as

$$V_q = U_{2q} / U_{1q} = \frac{K_{11}(\alpha_q) K_{23}(\alpha_q) - K_{12}(\alpha_q) K_{13}(\alpha_q)}{K_{13}(\alpha_q) K_{22}(\alpha_q) - K_{12}(\alpha_q) K_{23}(\alpha_q)} \quad (14)$$

$$W_q = U_{3q} / U_{1q} = \frac{K_{11}(\alpha_q) K_{23}(\alpha_q) - K_{12}(\alpha_q) K_{13}(\alpha_q)}{K_{12}(\alpha_q) K_{33}(\alpha_q) - K_{13}(\alpha_q) K_{23}(\alpha_q)} \quad (15)$$

According to Eqs. (13)-(15), the displacement ratios also have unique properties of

$$W_2 = -W_1 \quad W_4 = -W_3 \quad W_6 = -W_5 \quad (16)$$

$$V_2 = V_1 \quad V_4 = V_3 \quad V_6 = V_5$$

At this point, the displacement and stress at any point of a lamina are given as

$$[u_1, u_2, u_3] = \sum_{q=1}^6 [L, V_q, W_q] U_{1q} e^{ik(x_1 + \alpha_q x_3 - c_p t)} \quad (17)$$

Table 2 Material properties of carbon fiber reinforced epoxy laminate

$E_1$ (GPa)	$E_2$ (GPa)	$E_3$ (GPa)	$G_{12}$ (GPa)	$G_{13}$ (GPa)
175.9	8.73	8.73	4.49	4.49
$\nu_{12}$	$\nu_{13}$	$\nu_{23}$	Density (g/cm)	Thickness (mm)
0.34	0.34	0.28	1.576	0.191

$$[\sigma_{33}, \sigma_{13}, \sigma_{23}] = \sum_{q=1}^6 ik[D_{1q}, D_{2q}, D_{3q}]U_{1q}e^{ik(x_1 + \alpha_q x_3 - c_p t)} \quad (18)$$

where

$$D_{1q} = C_{13} + C_{36}V_q + C_{33}\alpha_q W_q \quad (19)$$

$$D_{2q} = C_{55}(\alpha_q + W_q) + C_{45}\alpha_q V_q \quad (20)$$

$$D_{3q} = C_{45}(\alpha_q + W_q) + C_{44}\alpha_q V_q \quad (21)$$

Due to the uniqueness of  $\alpha_q$ ,  $V_q$ , and  $W_q$ , the following properties are obtained

$$\begin{aligned} D_{12} &= D_{11} & D_{14} &= D_{13} & D_{16} &= D_{15} \\ D_{22} &= -D_{21} & D_{24} &= -D_{23} & D_{26} &= -D_{25} \\ D_{32} &= -D_{31} & D_{34} &= -D_{33} & D_{36} &= -D_{35} \end{aligned} \quad (22)$$

By applying the traction-free boundary conditions at the top and bottom surfaces of the laminates ( $x_3 = \pm h$ ) in Eq. (18), six equations in terms of the partial amplitudes  $U_{1q}$  are obtained. Applying the uniqueness properties of Eqs. (13), (16), and (22), the characteristic equation is derived to give nontrivial solutions of  $U_{1q}$

$$\begin{vmatrix} D_{11}E_1 & D_{11}\bar{E}_1 & D_{13}E_3 & D_{13}\bar{E}_3 & D_{15}E_5 & D_{15}\bar{E}_5 \\ D_{21}E_1 & -D_{21}\bar{E}_1 & D_{23}E_3 & -D_{23}\bar{E}_3 & D_{25}E_5 & -D_{25}\bar{E}_5 \\ D_{31}E_1 & -D_{31}\bar{E}_1 & D_{33}E_3 & -D_{33}\bar{E}_3 & D_{35}E_5 & -D_{35}\bar{E}_5 \\ D_{11}\bar{E}_1 & D_{11}E_1 & D_{13}\bar{E}_3 & D_{13}E_3 & D_{15}\bar{E}_5 & D_{15}E_5 \\ D_{21}\bar{E}_1 & -D_{21}E_1 & D_{23}\bar{E}_3 & -D_{23}E_3 & D_{25}\bar{E}_5 & -D_{25}E_5 \\ D_{31}\bar{E}_1 & -D_{31}E_1 & D_{33}\bar{E}_3 & -D_{33}E_3 & D_{35}\bar{E}_5 & -D_{35}E_5 \end{vmatrix} = 0 \quad (23)$$

where  $E_q = e^{ik\alpha_q h}$  and  $\bar{E}_q = E_q^{-1}$ . Recalling that  $E_q + \bar{E}_q = 2\cos(k\alpha_q h)$  and  $E_q - \bar{E}_q = 2i\sin(k\alpha_q h)$ , Eq. (23) is further simplified into two decoupled characteristic equations corresponding to the symmetric and anti-symmetric wave modes, respectively

$$S = D_{11}G_1 \cot(\gamma\alpha_1) + D_{13}G_3 \cot(\gamma\alpha_3) + D_{15}G_5 \cot(\gamma\alpha_5) = 0 \quad (24)$$

$$A = D_{11}G_1 \tan(\gamma\alpha_1) + D_{13}G_3 \tan(\gamma\alpha_3) + D_{15}G_5 \tan(\gamma\alpha_5) = 0 \quad (25)$$

where

$$\begin{aligned} G_1 &= D_{23}D_{35} - D_{25}D_{33} & G_3 &= D_{25}D_{31} - D_{21}D_{33} \\ G_5 &= D_{21}D_{33} - D_{23}D_{31} & \gamma &= 2\pi fh / c_p \end{aligned}$$

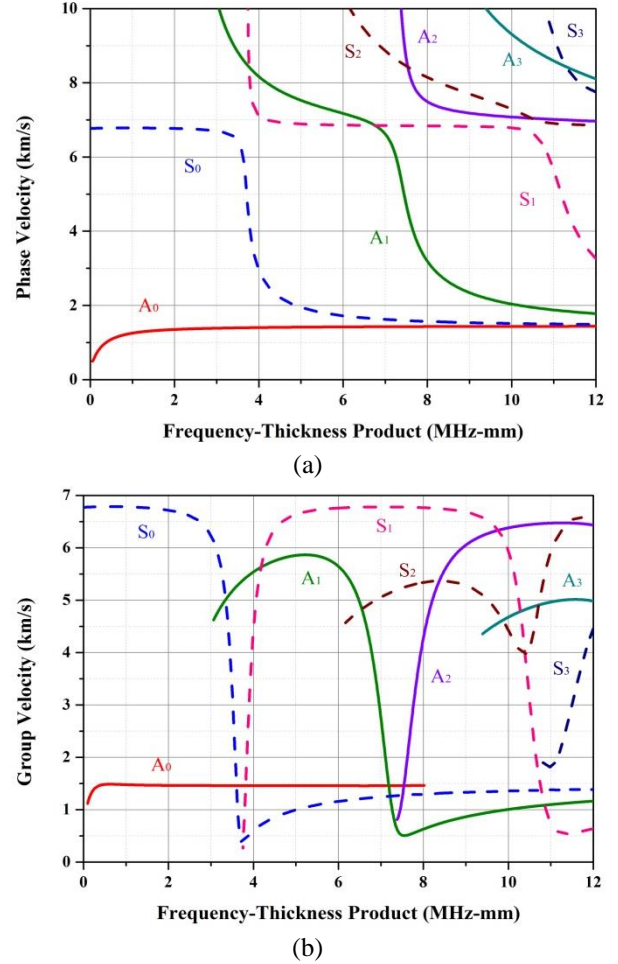


Fig. 3 Dispersion curve of  $[45/0/-45/90]_{2s}$  laminate: (a) phase velocity and (b) group velocity

For instance, the dispersion curves of phase and group velocities for  $[45/0/-45/90]_{2s}$  laminates are shown in Fig. 3.

The wave propagation direction is  $45^\circ$ , and the material properties of the laminate are given in Table 2.

### 3. Non-reflecting boundary

The Lamb waves are high-frequency vibrations that obey the equations in theory of elasticity. Adding the damping term in the wave equation can decrease the amplitude of vibration. To this end, non-reflecting boundaries are designed as damping frames to decrease the amplitude of waves at the plate edges.  $N$  frames are partitioned around the boundary, and the damping coefficient  $\alpha_n$  of each frame is defined as

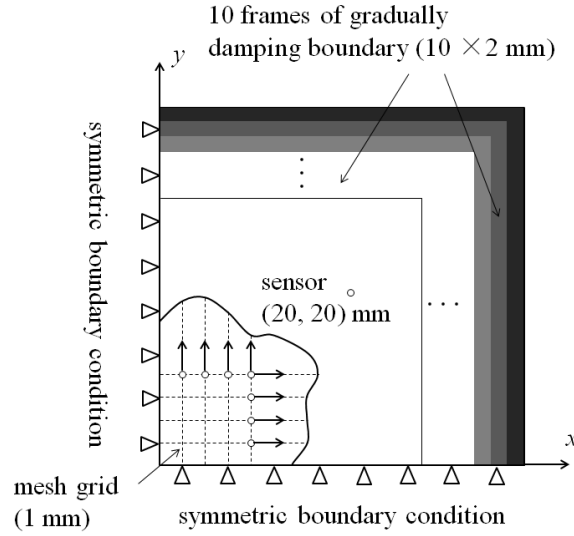


Fig. 4 Finite element modeling of non-reflecting boundaries

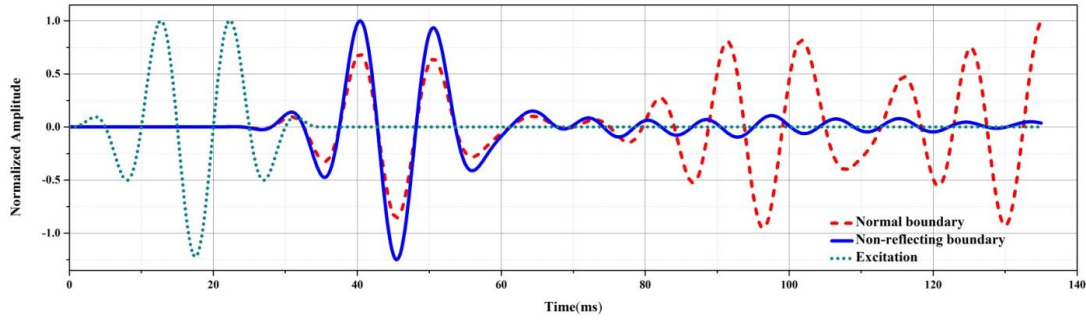


Fig. 5 Comparison of different boundaries

$$\alpha_n = \frac{\alpha_{\max} l_n^3}{\left(\sum_{n=1}^N l_n\right)^3} \quad (26)$$

where  $l_n$  is the length of the  $n$ -th frame, and  $\alpha_{\max}$  is the largest damping coefficient. These frames permit rapid damping growth while avoiding inter-frame reflection due to sudden damping changes.

A three-dimensional (3-D) FE model was built in ABAQUS to validate applicability of non-reflecting boundaries. Only a quarter of the plate ( $0.1 \times 0.1 \times 0.001$  m) was modeled, by considering its symmetry about the  $x$  and  $y$  axis (see Fig. 4). The model was discretized by  $1 \times 1$  mm C3D8R elements, and the time increment was  $2 \times 10^{-7}$  s was considered. The excitation  $x(t)$  was a tone burst with a central frequency of 100 kHz

$$x(t) = \sin(2\pi f_c t) \left[ 1 - \cos\left(\frac{2\pi f_c t}{3.5}\right) \right] \quad (27)$$

where  $f_c$  is the central frequency. This tone burst was applied as in-plane concentrated forces on the element nodes 4 mm away around the origin, assuming that most shear comes from the edges of piezoelectric disk. Ten damping frames were assigned at the plate edges with a

length of 2 mm and  $\alpha_{\max}$  was chosen as  $4 \times 10^6$ . The direct waves were extracted as the normalized out-of-plane displacement at (40, 40) mm, indicating that the boundary reflections (waves after 80  $\mu$ s) are effectively reduced, as shown in Fig. 5. In addition, the snapshots of the simulation with non-reflecting and normal boundaries are presented in Fig. 6 for the sake of comparison.

#### 4. Time-frequency analysis

In this section, two time-frequency analysis, i.e., the slant-stack (SL) transformation and the short-time Fourier transformation (STFT), are introduced, from which the phase and group velocities are calculated, respectively. By applying these transformations, the direct waves are used to characterize the dispersion of Lamb waves.

##### 4.1 Phase velocity via SL transformation

SL transformation can be adopted to measure the phase velocity of Lamb waves. For simplicity of explanation, the Lamb waves are assumed to be non-attenuating during propagation. After transmitting an excitation  $s$  with the frequency of interest, the direct wave  $y$  at location  $x$  is given as

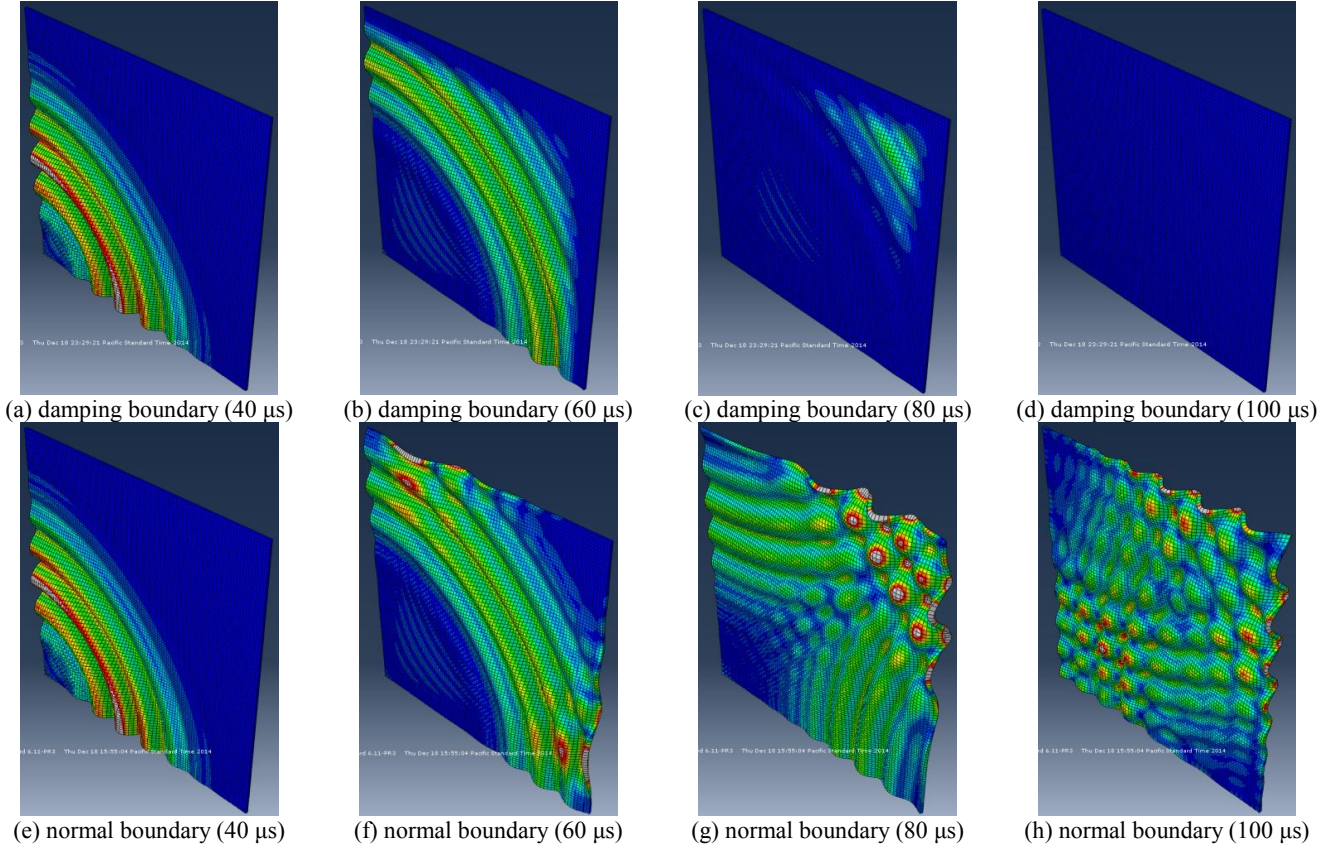


Fig. 6 Snapshots of the FE simulation

$$y(x, t) = s(t) * \delta\left(t - \frac{x}{c_p}\right) = s\left(t - \frac{x}{c_p}\right) \quad (28)$$

when the responses of excitation are recorded by a series of transducers located in a linear configuration along the wave propagation path (see Fig. 7). In reference to the first transducer (the one closest to the excitation), the direct wave received by the  $n$ -th transducer gains a time delay

$$y(x_n, t, c) = s\left(t - \frac{x_n}{c_p} + \frac{x_n}{c}\right) \quad (29)$$

where  $c$  is the shifting parameter. When the shifting parameter  $c$  equals the phase velocity  $c_p$ ,  $y$  reaches the maximum. Then, the direct waves received by different transducers are shifted in amounts of  $c$  and summed up to index  $sl$

$$sl(t, c) = \sum_{n=1}^N s\left(t - \frac{x_n}{c_p} + \frac{x_n}{c}\right) \quad (30)$$

where  $N$  is the total number of transducers. By changing the parameters  $t$  and  $c$ , a contour is generated to show the variance of  $sl$  with respect to time and velocity. For a specific time, the velocity corresponding to the maximum of  $sl$  on this contour indicates the measured phase velocity. By performing Fourier transformation regarding the time variable  $t$ , the contour is converted to the frequency-velocity domain

$$SL(\omega, c) = F\left[\sum_{n=1}^N s\left(t - \frac{x_n}{c_p} + \frac{x_n}{c}\right)\right] \quad (31)$$

where  $F$  represents the Fourier transformation. The energy distribution with respect to frequency  $\omega$  and phase velocity  $c$  should be consistent with the analytical phase velocity of the Lamb wave.

#### 4.2 Group velocity via STFT

STFT can be adopted to measure the group velocity of Lamb waves. STFT divides the direct wave into short segments of equal length in the time domain and then performs a Fourier transformation on each segment separately. By determining the frequency for each segment, STFT represents the direct wave in the time-frequency domain as follows

$$STFT\{x(t)\}(\tau, \omega) = \int_{-\infty}^{\infty} x(t)w(t-\tau)e^{-j\omega t} dt \quad (32)$$

where  $w(t)$  is the window function. The energy distribution in the time-frequency domain should be consistent with the analytical group velocity of the Lamb wave.

Since STFT provides sinusoid basis for signal decomposition, it is essentially suitable to analyze direct waves excited by a chirp signal (the excitation in following sections), compared with the wavelet and Hilbert-Huang transformations.

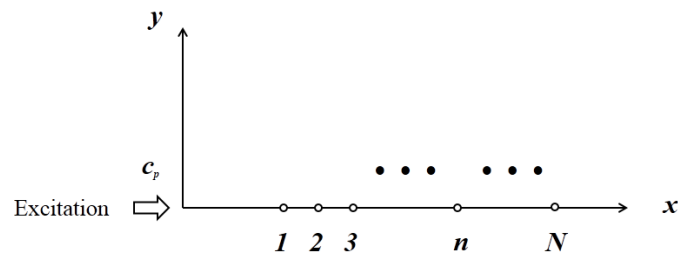


Fig. 7 Illustration of the SL transformation

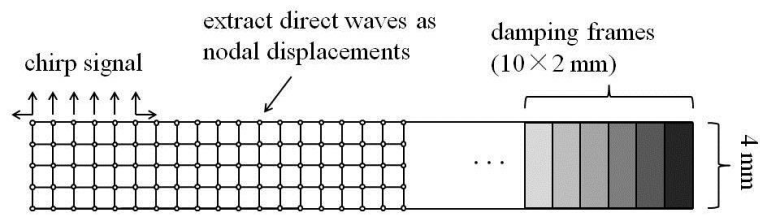


Fig. 8 2-D modeling of an aluminum plate

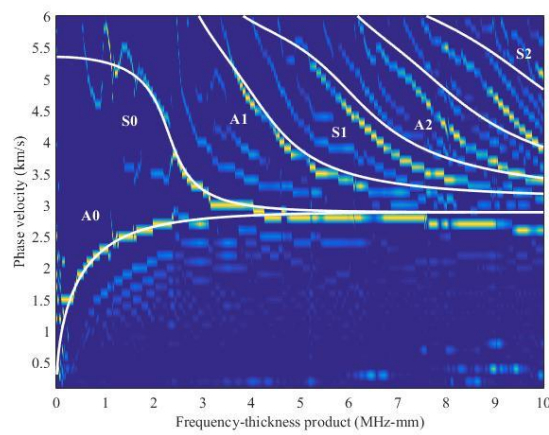


Fig. 9 Dispersion curve of phase velocity in aluminum plate

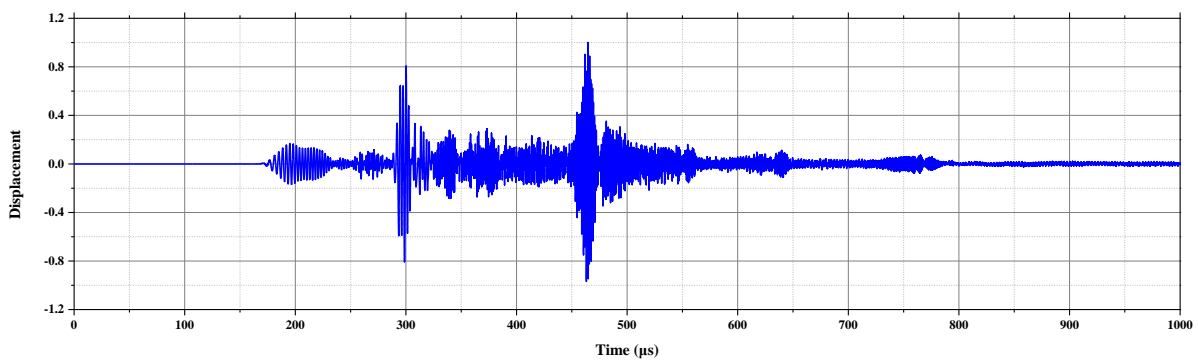


Fig. 10 Signal at 0.9 m from the left end

## 5. FE simulation

The non-reflecting boundaries developed in Section 3 are applied in a two-dimensional (2-D) FE model to simulate propagation of Lamb waves. After the boundary reflections are effectively decreased, the direct waves are clearly extracted. By applying the time-frequency analysis described in Section 4, the dispersion curves of phase and group velocities are characterized in contours and compared with the analytical solutions derived in Section 2.

### 5.1 Description of FE model

Since the shear horizontal wave remains decoupled in addition to the longitudinal and shear vertical waves in isotropic material, the plane strain condition was applied to facilitate the development of a 2-D FE model in the longitudinal-thickness plane. The mesh size and time increment were set to 0.2 mm and  $1 \times 10^{-8}$  s, respectively.

A chirp signal whose frequency swept from 0 to 10 MHz in  $1 \times 10^{-4}$  s was applied as the nodal displacement to input various frequency contents (see Fig. 8). Ten frames of the damping boundary were assigned on the right end of a 4 mm-thick aluminum plate to absorb reflection. Direct waves were extracted as out-of-plane displacements at the points 30 mm to 60 mm from the left end with a space of 0.2 mm.

### 5.2 Dispersion curve of phase velocity

All the direct waves are subjected to SL transformation to present a contour in the frequency-velocity domain. The energy distribution on this frequency-velocity contour compares well with the analytical solutions, as demonstrated in Fig. 9.

### 5.3 Dispersion curve of group velocity

Due to the dispersive group velocity, different frequency contents reach the transducer at different time. By applying STFT to the direct wave 0.9 m from the left end (see Fig. 10), the time of arrival of a specific frequency can be represented on the time-frequency contour.

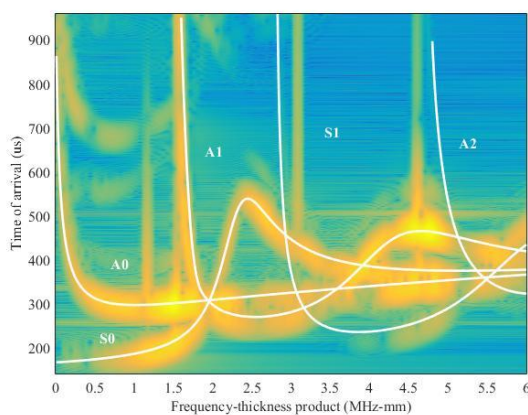


Fig. 11 Dispersion curve of group velocity in aluminum plate

For comparison, the analytical dispersion curves of group velocity are converted to the time-frequency domain and plotted on the STFT contour (see Fig. 11), demonstrating that the energy distribution along this contour agrees well with the analytical solutions.

## 6. Experiment

In this section, the group velocities of Lamb waves are measured through experiments on aluminum and laminated plates, respectively. Both plates are sealed by damping clay to absorb waves at plate edges. By applying STFT to the direct waves, the group velocities are characterized in contours and compared with the analytical solutions.

### 6.1 Experimental setup

Two experiments were conducted to measure the group velocities of the Lamb waves on the isotropic and laminated plates. To keep the direct waves clean, damping clay was sealed at the plate edges to absorb the boundary reflections. A chirp signal, whose frequency rose from 1  $\mu$ Hz to 1 MHz in 0.1  $\mu$ s, was generated by the Agilent<sup>®</sup> 3325A waveform generator. The voltage of the chirp signal was amplified to 200 Vpp by the PINTEK<sup>®</sup> HA-405 high voltage amplifier. A signal from the monitoring terminal of the amplifier with a -40 dB attenuation was input to the Agilent<sup>®</sup> DSO7034B oscilloscope as a trigger. Once the transmitter was excited, the oscilloscope recorded the voltage variation of the receiver in a 1.8  $\mu$ s period with a sampling frequency of 20 MHz. The recorded signals were then subjected to the STFT to characterize the dispersion of group velocity on a time-frequency contour.

### 6.2 Dispersion in aluminum plate

The group velocity was measured on an  $800 \times 800 \times 3$  mm aluminum plate (see Fig. 12) whose material properties are shown in Table 1. Two piezoelectric disks were mounted at the upper corners of the plate, functioning as a transmitter and receiver, respectively.

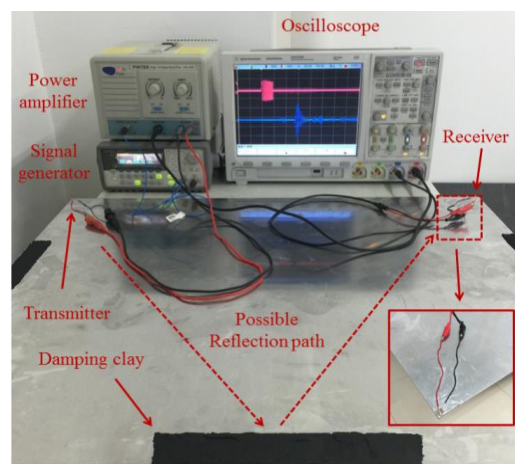


Fig. 12 Group velocity measurement in aluminum plate

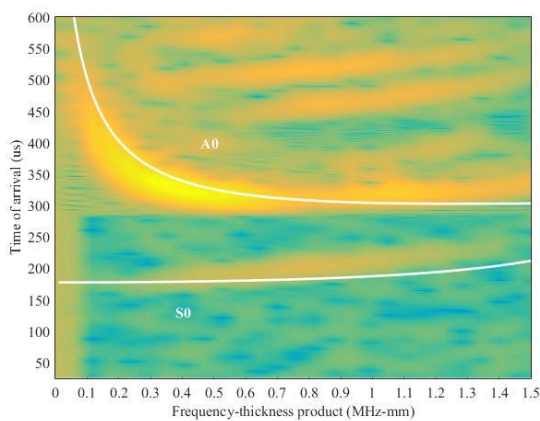


Fig. 13 Time-frequency contour in the aluminum plate

The time-frequency contour of this signal is produced by STFT and then compared with the analytical solutions, as shown in Fig. 13. The energy distribution is in accordance with the analytical solutions.

### 6.3 Dispersion in laminated plate

A similar measurement was conducted on a  $590 \times 590 \times 3$  mm  $[45/0/-45/90]_{2s}$  laminated plate (see Fig. 14). The transmitter and receiver were mounted at the diagonal corners of the plate to measure the Lamb wave propagating at  $45^\circ$ . The output cables, which were used to excite the transmitter, were wrapped by foil tape and connected to the grounding terminal of the oscilloscope to alleviate the electromagnetic crosstalk in the received signals.

The time-frequency contour of the received signal along with the analytical solutions is plotted in Fig. 15, and a good correlation is observed.

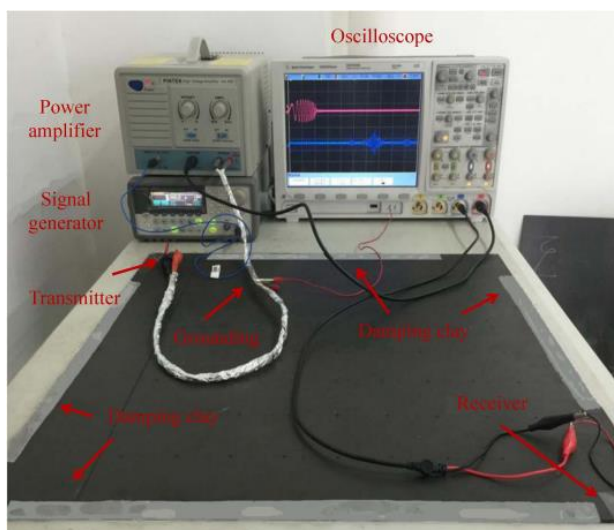


Fig. 14 Group velocity measurement in laminated plate

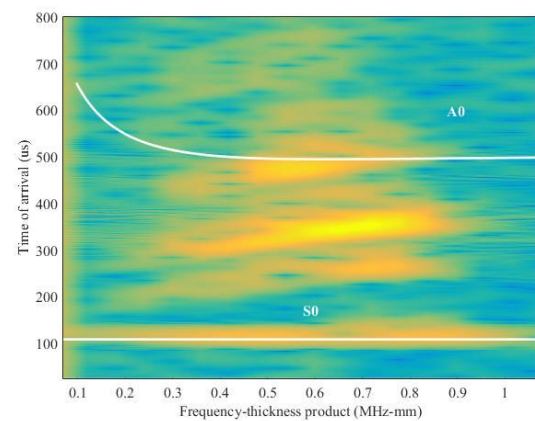


Fig. 15 Time-frequency contour in the laminated plate

## 7. Conclusions

To facilitate the time-frequency characterization of Lamb wave dispersion, the non-reflecting boundaries are developed in both numerical and experimental cases as damping frames and damping clay, respectively. These damping boundaries are capable of absorbing waves at plate edges and accordingly purifying the wave field of interest. By applying time-frequency analysis to the direct waves obtained from the purified wave field, Lamb wave dispersion can be characterized in a way that has strong accordance with the analytical solutions. Both the numerical and experimental results obtained from both isotropic and laminated materials demonstrate that the combination of a non-reflecting boundary and time-frequency analysis is a feasible and reliable way to evaluate elastic waves and can be extended to more complex scenarios.

## Acknowledgements

The research described in this paper was financially supported by the National Natural Science Foundation of China (Grant No.: 51609148) and China Postdoctoral Science Foundation (Grant No.: 2017M621609).

## References

- Ambrozinski, L., Piwakowski, B., Stepinski, T. and Uhl, T. (2014), "Evaluation of dispersion characteristics of multimodal guided waves using slant stack transform", *NDT & E Int.*, **68**, 88-97.
- Drozd, M., Moreau, L., Castaigns, M., Lowe, M.J.S. and Cawley, P. (2006), "Efficient numerical modelling of absorbing regions for boundaries of guided waves problems", *AIP Conference Proceedings*, **820**(1), 126-133.
- Giurgiutiu, V. (2011), "Piezoelectric wafer active sensors for structural health monitoring of composite structures using tuned guided waves", *J. Eng. Mater. Technol.*, **133**(4), 041012-041012.
- He, C., Liu, H., Liu, Z. and Wu, B. (2013), "The propagation of coupled Lamb waves in multilayered arbitrary anisotropic composite laminates", *J. Sound Vib.*, **332**(26), 7243-7256.
- Hong, M., Su, Z., Wang, Q., Cheng, L. and Qing, X. (2014),

- “Modeling nonlinearities of ultrasonic waves for fatigue damage characterization: theory, simulation, and experimental validation”, *Ultrasonics*, **54**(3), 770-778.
- Hosseini, S.M.H., Ducek, S. and Gabbert, U. (2013), “Non-reflecting boundary condition for Lamb wave propagation problems in honeycomb and CFRP plates using dashpot elements”, *Compos. Part B: Eng.*, **54**, 1-10.
- Liu, G.R. and Quek Jerry, S.S. (2003), “A non-reflecting boundary for analyzing wave propagation using the finite element method”, *Finite Elem. Anal. Des.*, **39**(5-6), 403-417.
- Niethammer, M., Jacobs, L.J., Qu, J. and Jarzynski, J. (2000), “Time-frequency representation of Lamb waves using the reassigned spectrogram”, *J. Acoust. Soc. Am.*, **107**(5), 19-24.
- Pant, S., Laliberte, J., Martinez, M. and Rocha, B. (2014), “Derivation and experimental validation of Lamb wave equations for an n-layered anisotropic composite laminate”, *Compos. Struct.*, **111**, 566-579.
- Poddar, B. and Giurgiutiu, V. (2016a), “Complex modes expansion with vector projection using power flow to simulate Lamb waves scattering from horizontal cracks and disbonds”, *J. Acoust. Soc. Am.*, **140**(3), 2123-2133.
- Poddar, B. and Giurgiutiu, V. (2016b), “Scattering of Lamb waves from a discontinuity: an improved analytical approach”, *Wave Motion*, **65**, 79-91.
- Qiu, L., Liu, M., Qing, X. and Yuan, S. (2013), “A quantitative multidamage monitoring method for large-scale complex composite”, *Struct. Health Monit.*, **12**(3), 183-196.
- Rose, J.L. (2004), “Ultrasonic waves in solid media”, Cambridge university press.
- Shen, Y. and Giurgiutiu, V. (2015), “Effective non-reflective boundary for Lamb waves: theory, finite element implementation, and applications”, *Wave Motion*, **58**, 22-41.
- Tao, C., Ji, H., Qiu, J., Zhang, C., Wang, Z. and Yao, W. (2017), “Characterization of fatigue damages in composite laminates using Lamb wave velocity and prediction of residual life”, *Compos. Struct.*, **166**, 219-228.
- Wang, L. and Yuan, F.G. (2007), “Group velocity and characteristic wave curves of Lamb waves in composites: modeling and experiments”, *Compos. Sci. Technol.*, **67**(7-8), 1370-1384.
- Wang, Q., Yuan, S.F., Hong, M. and Su, Z.Q. (2015), “On time reversal-based signal enhancement for active lamb wave-based damage identification”, *Smart Struct. Syst.*, **15**(6), 1463-1479.
- Wang, Z. and Qiao, P. (2017), “Backward wave separation method in a single transmitter and multi-receiver sensor array for improved damage identification of two-dimensional structures”, *Int. J. Damage Mech.*, **26**(2), 229-250.
- Wang, Z., Qiao, P. and Shi, B. (2016), “Application of soft-thresholding on the decomposed Lamb wave signals for damage detection of plate-like structures”, *Measurement*, **88**, 417-427.
- Wang, Z., Qiao, P. and Shi, B. (2017), “A comprehensive study on active Lamb wave-based damage identification for plate-type structures”, *Smart Struct. Syst.*, **20**(6), 759-767
- Yi, T.H., Li, H.N. and Gu, M. (2011), “Characterization and extraction of global positioning system multipath signals using an improved particle-filtering algorithm”, *Measurement Sci. Technol.*, **22** (7).
- Yi, T.H., Li, H.N. and Sun, H.M. (2013), “Multi-stage structural damage diagnosis method based on "energy-damage" theory”, *Smart Struct. Syst.*, **12**(3-4), 345-361.

## Appendix A

$$A_1 = (-c^2 C_{33} C_{44} \rho - c^2 C_{33} C_{55} \rho - c^2 C_{44} C_{55} \rho + c^2 C_{45}^2 \rho + C_{11} C_{33} C_{44} - C_{13}^2 C_{44} + 2C_{13} C_{36} C_{45} - 2C_{13} C_{44} C_{55} + 2C_{13} C_{45}^2 - 2C_{16} C_{33} C_{45} + C_{33} C_{55} C_{66} - C_{36}^2 C_{55}) / \Delta$$

$$A_2 = (c^4 C_{33} \rho^2 + c^4 C_{44} \rho^2 + c^4 C_{55} \rho^2 - c^2 C_{11} C_{33} \rho - c^2 C_{11} C_{44} \rho + c^2 C_{13}^2 \rho + 2c^2 C_{13} C_{55} \rho + 2c^2 C_{16} C_{45} \rho - c^2 C_{33} C_{66} \rho + c^2 C_{36}^2 \rho + 2c^2 C_{36} C_{45} \rho - c^2 C_{44} C_{55} \rho + c^2 C_{45}^2 \rho - c^2 C_{55} C_{66} \rho + C_{11} C_{33} C_{66} - C_{11} C_{36}^2 - 2C_{11} C_{36} C_{45} + C_{11} C_{44} C_{55} - C_{11} C_{45}^2 - C_{13}^2 C_{66} + 2C_{13} C_{16} C_{36} + 2C_{13} C_{16} C_{45} - 2C_{13} C_{55} C_{66} - C_{16}^2 C_{33} + 2C_{16} C_{36} C_{55}) / \Delta$$

$$A_3 = (-c^6 \rho^3 + c^4 C_{11} \rho^2 + c^4 C_{55} \rho^2 + c^4 C_{66} \rho^2 - c^2 C_{11} C_{55} \rho - c^2 C_{11} C_{66} \rho + c^2 C_{16}^2 \rho - c^2 C_{55} C_{66} \rho + C_{11} C_{55} C_{66} - C_{16}^2 C_{55}) / \Delta$$

$$\Delta = C_{33} C_{44} C_{55} - C_{33} C_{45}^2$$